Robotics and Computer–Integrated Manufacturing 94 (2025) 102975

Contents lists available at ScienceDirect

Robotics and Computer-Integrated Manufacturing

journal homepage: www.elsevier.com/locate/rcim

Macro-mini collaborative manipulator system for welding in confined environments

Erhui Sun [a,b], Josue Camacho-Arreguin [a], Junfu Zhou [a], Max Liebenschutz-Jones [a], Tianyi Zeng [a], Max Keedwell [c], Dragos Axinte [a], Andy Norton [b], Abdelkhalick Mohammad [a,*]

[a] Rolls-Royce UTC in Manufacturing and On-Wing Technology, University of Nottingham, Nottingham, UK, NG8 1BB
[b] Rolls-Royce plc, Derby, UK, DE24 8BJ
[c] Rolls-Royce plc, Bristol, UK, BS34 7QE

ARTICLE INFO

Keywords:
Welding
Robotic welding
TIG welding
Manipulator
Robot
Confined environment

ABSTRACT

Welding plays an important role in a wide range of industries, including aviation, aerospace, automobile manufacturing, and nuclear and chemical plants, all of which contain critical industrial assets. However, confined spaces and complex structures in these environments severely restrict the accessibility and functionality of in-situ welding tasks. Therefore, to enable welding operations in constrained spaces, a macro-mini collaborative manipulator system with multiple Degrees of Freedom (multi-DoF) is proposed in this paper. The collaborative system consists of a 6-DoF macro robotic arm and a novel 2-DoF slim mini manipulator. The macro manipulator (i.e., the robotic arm) provides large-scale movement to position the slim mini manipulator within confined environments. The slim mini manipulator, which features a novel serial mechanism, then adjusts and controls the pose of the end-effector (welding torch) to perform welding tasks in spaces that the macro manipulator cannot access. Given the novel design of the mini manipulator, kinematic and Jacobian modelling have been developed to enable intimate and accurate control of the collaborative welding system. The collaboration between the macro and mini manipulators occurs not only for individual movements but also at the level when compensatory movements are performed on each system to enable error compensation for the end-effector (i.e., welding torch). Finally, validation experiments of the collaborative manipulator system have been conducted in confined scenarios to verify its functionality and performance.

1. Introduction

Welding is a process of high use in various industries because of its simplicity and well-defined quality of methods for machining, such as repair and assembly [1]. Although welding is effortless to be performed in easy-to-access workplaces by human operators, the welding quality of the manual welding process highly relies on specialised and experienced human welders [2]. In order to accomplish better consistency, higher repeatability and faster welding efficiency in a welding process, automatic welding (e.g., robot-assisted welding) presents a possibility [3]. With the recent progress in the fields of robotics, computer vision, artificial intelligence, sensors and control theory [4,5], the transition from human-based welding to automatic welding has been achieved [6]. Automatic welding allows robots to learn and imitate the welding behaviours performed by skilled human operators, which makes robot-assisted welding widely adopted in industrial areas [7,8].

However, the situation becomes more demanding when machining operation needs to be performed in narrow and constrained spaces [9]. While this is possible by human operators, this requires skills and sometimes it requires the human operators to subject themselves to harsh/hazardous environments [10]. For the case of accessing confined spaces, conventional robots are also difficult to utilise because of their large size and difficulty in avoiding collisions [11]. End-effectors or additional manipulators that are mounted at the end of the conventional robots might be a way forward [12].

Based on this idea, end-effectors/mini-manipulators mounted on macro robots for the polishing, drilling and milling processes have been reported [13]. However, most state-of-the-art end-effectors focus on the machining process, such as position accuracy or force control, to achieve a good machining quality [14]. However, for access to confined spaces,

* Corresponding author.
E-mail address: abd.moahmmad1@nottingham.ac.uk (A. Mohammad).

https://doi.org/10.1016/j.rcim.2025.102975
Received 28 August 2024; Received in revised form 16 January 2025; Accepted 2 February 2025
Available online 9 February 2025

the aforementioned end-effectors haven't been considered and paid attention to. For example, Mohammad etc. designed a force-controlled end-effector mounted on an industrial robot to achieve an automated polishing process [13]. However, the diameter of the end-effector is comparable to the size of the industrial robot, making it difficult to access confined spaces.

For the implementation of robotic welding, a conventional approach is to use a 6-DoFs robot arm with a welding torch mounted at the end-effector, such as Tungsten Inert Gas (TIG) welding [15]. In [16], a detailed configuration setup indicates a typical configuration for this approach, where the robotic arm (e.g. ABB and KUKA, etc.) and the welding torch are combined with a series of sensors (e.g., vision sensor and arc seam tracking sensor, etc.), welding machine and wire feeder to build a welding system. Therefore, due to confined spaces and complex structures in some application scenarios (e.g., gas turbine engines and pipelines, etc.), conventional robotic welding systems are not only challenging to access repair positions, but also difficult to adjust their pose within limited spaces, which makes the in-situ welding process impossible to be achieved.

For the conventional robotic welding system generically depicted in Fig. 1a), the robot provides speed and position control for the end-effector (i.e., welding torch), which can achieve good welding quality and highly efficient operation in open areas. However, the rigid welding torch used in the robotic welding system severely affects its flexibility when accessing confined spaces, as shown as a generic example in Fig. 1b). During the welding process in constrained spaces, the conventional welding torch may cause collision/ interference problems within the surroundings and the workpiece. Although the collision problem may be partially solved by changing welding heads with different angles in some scenarios, it is difficult to achieve a continuous welding path which affects the final welding quality. In the meantime, frequent changes of the welding head are time-consuming for the welding process.

To solve the problem, new concepts of mini manipulators with a slim size (high length-to-width ratio) need to be proposed. As generically shown in Fig. 1c), a novel concept of a slim mini manipulator is mounted on the macro manipulator directly, which enables the welding head more DoFs to move freely and overcome the geometrical constraints of the workspace. The torch head can adjust its position and orientation independently to achieve a continuous welding path and avoid collision within confined spaces in real-time.

For the macro-mini collaborative manipulator system, an interesting topic here is how the conventional robot will interact and collaborate with the mini manipulator mounted at its end. If the mini manipulator replicates the structure of a robot over a serial or parallel kinematic structure, well-documented models for such configuration exist [17,18]. Therefore, the integration of the control is relatively straightforward [19]. However, if a new configuration of the mini manipulator is introduced, an interesting task would be how to integrate the two systems to work collaboratively. This collaboration is not only related to the position but also interesting in how to make compensation.

Hence, the proposed collaborative system aims for machining operations in confined environments with the following contribution: (1) A novel design of a slim mini manipulator for controlling and adjusting end-effectors (e.g., welding torch) in confined spaces; (2) Modelling and control of the proposed mini manipulator to accomplish position and speed control; And (3) the feasibility demonstration of the macro-mini welding system by achieving collaborative welding tests in a confined environment.

2. Novel design of the macro-mini manipulator for accessing confined spaces

In this section, the novel concept and design of the macro-mini collaborative manipulator welding system for confined environments are proposed and presented. Firstly, the general concept of the novel manipulator system is introduced by presenting it in a confined workspace scenario (e.g., part of a turbine engine). Secondly, the collaborative mechanism is presented to ensure the welding functionality of the macro-mini manipulator system. Finally, the mini manipulator is presented and explained in detail, which has 2-DoF movements driven by two slider-crank mechanisms in series.

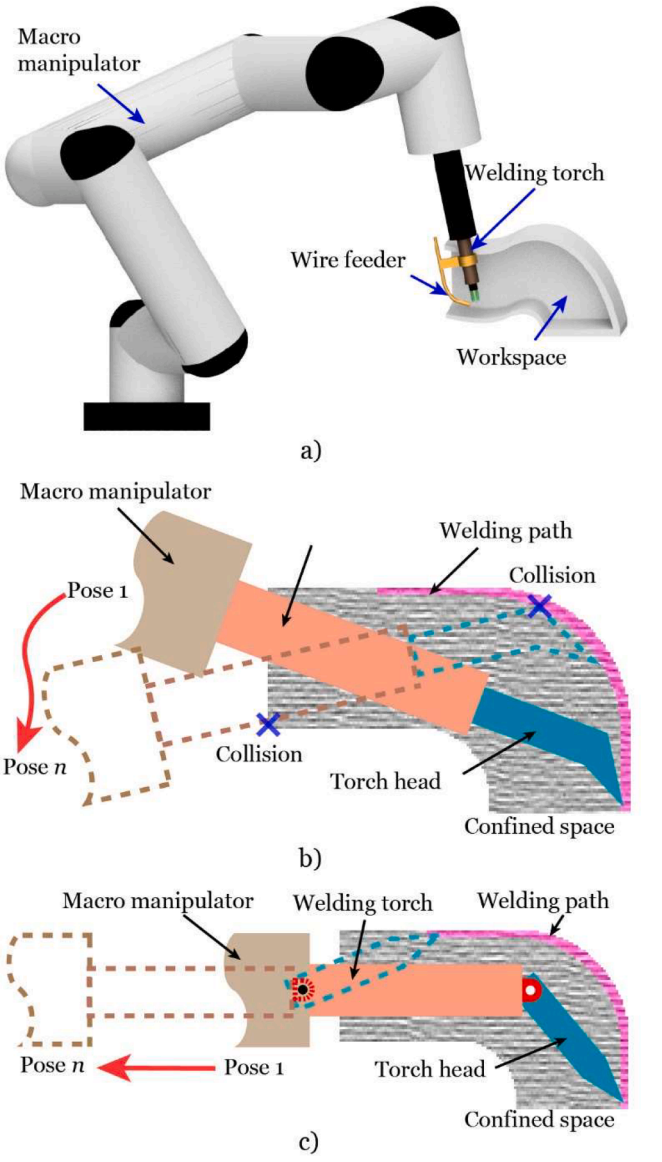

Fig. 1. Example of robotic welding system and its potential problem for access to confined spaces. a) An example of the conventional robotic welding system with a rigid welding torch is trying to access a confined space; b) The rigid welding torch on the robotic arm makes it difficult to achieve a continuous welding path without collision in confined spaces. c) One potential solution is enabling the welding torch more DoFs to make it flexible to access confined spaces and achieve the desired welding path.

2.1. System concept

As shown in Fig. 2, the macro-mini collaborative manipulator system is achieved when the slim mini manipulator of a novel design is attached to a macro manipulator (off-the-shelf 6-DoF robot), which enables the access of the end-effector (welding torch) into constraint spaces [20]. The macro manipulator provides large-scale movement and carries the mini manipulator to reach inside the confined space, where the target position is located. The novel mini manipulator employs two motors to

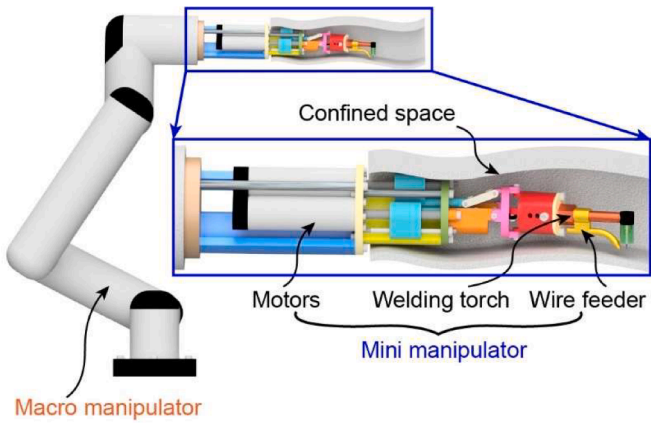

Fig. 2. A general concept of the collaborative manipulator which consists of a macro manipulator and mini manipulator is proposed to access a confined environment and accomplish machining tasks (e.g., welding). For the slim mini manipulator, an extra 2-DoF is enabled to the end-effector (e.g., welding torch) for access to confined spaces without collision. The macro manipulator not only provides large-scale movement for the collaborative welding system but also offers compensation for the movement of the slim mini manipulator.

manipulate the welding torch to achieve 2-DoF movement. The extra DoFs of the mini manipulator enable the end-effector (welding torch) to achieve the desired poses in confined spaces without necessarily moving the macro manipulator (the robot), which helps collision avoidance and motion planning of the welding process. Furthermore, combined with the compensation from the macro manipulator, the welding torch can achieve enhanced manoeuvrability within space constraints.

2.2. Collaborative mechanism of macro-mini manipulator

One advantage of the collaborative manipulator system is that the movement of the end-effector (i.e., welding torch) can be adjusted and optimised in real-time to achieve the desired welding path while keeping safe clearances within confined spaces.

The collaborative system has three operation modes, i.e., 1) the macro manipulator actuates only; 2) the slim mini manipulator actuates only; and 3) the collaborative movement with both the macro and the mini manipulators.

1) For the movement from the external open space to the internal confined space, a large-scale movement is required, as shown in Fig. 3a). In this case, the macro manipulator plays a dominant role in executing the desired movement.
2) However, when the collaborative manipulator system executes tasks within the internal confined space, the small-scale movement accomplished by the mini manipulator takes the dominant place, as shown in Fig. 3b). The mini manipulator has two rotation joints driven by two motors, which can achieve 2-DoF movement for the welding torch, enabling the welding torch to adjust its orientation and position in real-time. In this way, the potential collision between the end-effector (welding torch) and the constraint space will be avoided and a continuous welding movement can be achieved.
3) However, with the lack of freedom for linear movements, the mini manipulator cannot achieve 6-DoF movements without compensations. Therefore, the macro manipulator is required to provide compensations for the movement of the mini manipulator when necessary, as shown in Fig. 3c). In this way, the essence of collaboration between the macro manipulator and the mini manipulator is revealed.

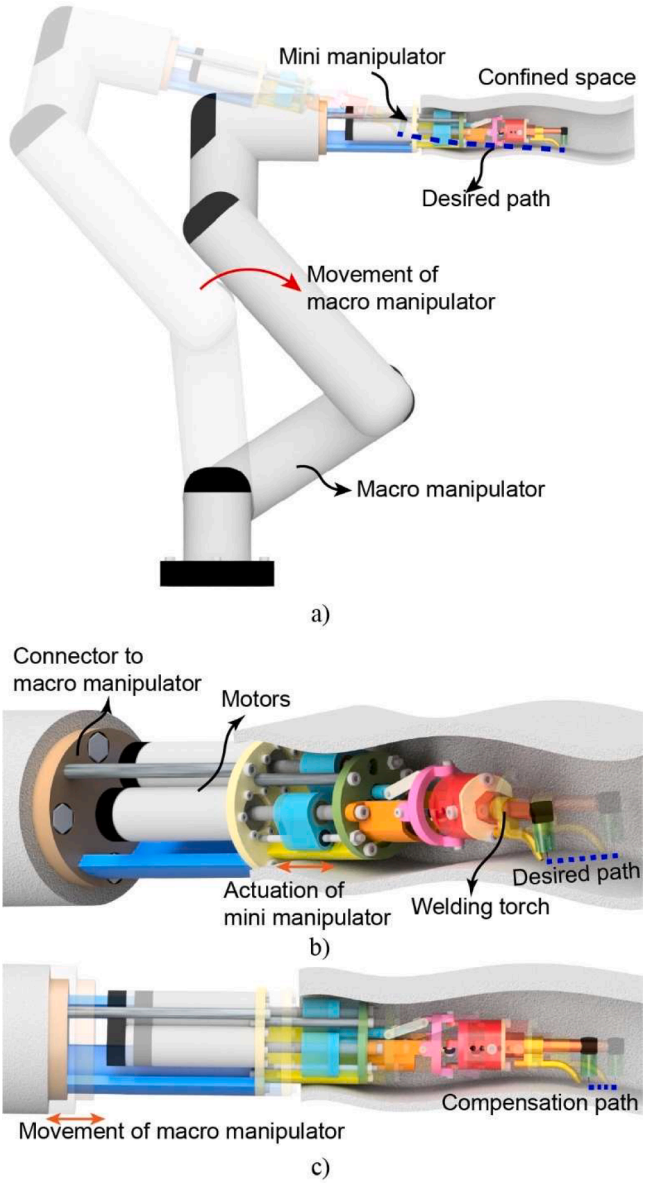

Fig. 3. Collaborate movements of the macro-mini manipulator. a) Large-scale movement of the *m*acro-mini manipulator from the externally confined space to the internally confined space; b) Small-scale movement of the collaborative manipulator within the confined internal space. c) Compensation movement of the macro-mini collaborative manipulator within the confined internal space to adjust the welding torch.

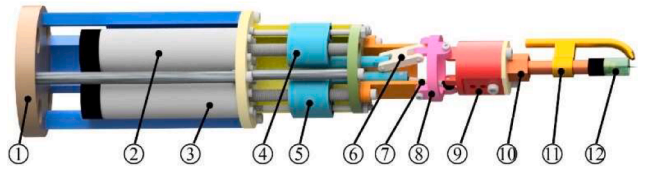

Fig. 4. Detailed description of the mini manipulator which manipulates the welding torch to achieve 2-DoF movement in confined environments. ① connector for adapting to the macro manipulator (e.g., UR, KUKA, ABB, etc.); ② LSC motor; ③ USC motor; ④ LSC slider; ⑤ USC slider; ⑥ LSC connecting link rod; ⑦ USC connecting link rod; ⑧ LSC rotational crank; ⑨ USC rotational crank (torch holder); ⑩ welding torch; ⑪ wire feeder; ⑫ torch head.

2.3. Design details of the mini manipulator

As shown in Fig. 4, the mini manipulator utilises two Direct Current (DC) motors to drive two slider-crank linkages (i.e., Lower Slider-Crank (LSC) linkage and Upper Slider-Crank (USC)) linkage separately, which manipulate the welding torch to accomplish 2-DoF movements. For conventional serial manipulators/robots, robot actuators are usually embedded into the robot joints themselves. Although this is a straightforward and simple configuration, it makes robots and joints bulky and difficult to access in constrained environments. Therefore, to make the mini manipulator slim and flexible for confined spaces, the motors/actuators of the mini manipulator are extracted from joints and moved to the manipulator's bottom. With this configuration, two slider-crank linkages are utilised to connect the actuators and joints to give proper driven forces.

Hence, the mini manipulator consists of a universal connector (①), two motors (② and ③), two slider-crank linkages (including two sliders ④ and ⑤, two link rods ⑥ and ⑦, two rotational cranks ⑧ and ⑨), a customised welding torch (⑩), a wire feeder (⑪) and a torch head (⑫). The universal connector (①) is used to attach the mini manipulator to a macro manipulator (e.g., a robotic arm). For the two slider-crank linkages, each contains three moving components with an offset configuration as follows (taking the LSC as an example):

1) a linear slider (④) which is connected to the motor (②) directly through a nut on a screw shaft to provide a linear driving force for the slider-crank linkage.
2) a rotational crank (⑧) which works as an output crank to convert the linear movement of the slider to rotation movement.
3) a connecting rigid link rod (⑥) which connects the slider and the rotational crank/ torch holder.

The two slider-crank linkages are connected in series to manipulate the welding torch for adjusting its pose in real-time.

2.4. Mini manipulator hardware integration and control system

2.4.1. Bespoke welding torch

To cater to the needs of operators to hold the welding torch ergonomically, off-the-shelf welding torches are usually equipped with a large and long handle, of which the size severely affects their flexibility in confined environments. To enable the mini manipulator to operate flexibly within constrained spaces, a miniaturised welding torch is customised based on a standard handheld welding torch, so that it can be mounted on the mini manipulator to access constraint spaces, as shown in Fig. 5a).

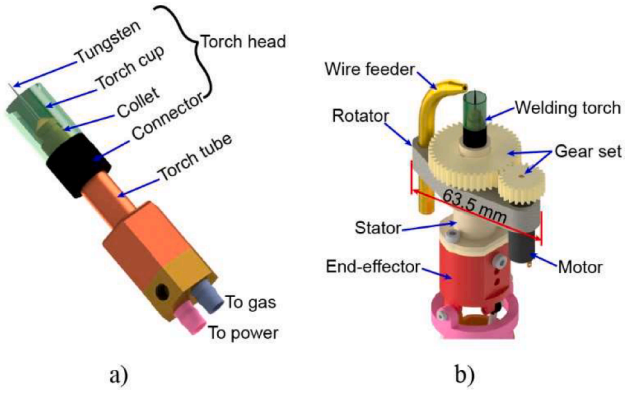

Fig. 5. Redesign of bespoke welding torch for the mini manipulator. a) Welding torch redesign based on the off-the-shelf handheld welding torch by truncating the handle and handle bushing; b) Rotation mechanism for the wire feeder to adjust the wire feeding direction in real-time.

2.4.2. Welding wire adjustment mechanism

For conventional robotic welding systems, they usually are equipped with a fixed wire feeder, attached to a fixed welding torch. Thus, the orientation of the wire feeder can be adjusted by the last joint of the macro robot (i.e., UR robot) advance to make sure that wire is always fed into the front of the welding direction while still keeping the TCP position of the welding torch. However, the extra 2-DoF for the welding torch and attached wire feeder adds another layer of complexity to the wire feeder control. When there is no tilt movement for the welding torch (i.e., joint rotation angle $\theta_1 = 0$ and $\theta_2 = 0$), it is possible to use the last joint of the macro robot to control the wire feeder, similar to the conventional robotic welding system. However, it is impossible to do so when there is tilt movement of the welding torch (i.e., $\theta_1 \neq 0$ or $\theta_2 \neq 0$) while still keeping the TCP position. Furthermore, although the problem can be solved if more joints of the UR robot are involved, it will increase the possibility of robot collision with constrained surrounding in confined environments.

Therefore, a novel rotation mechanism for the wire feeder is designed and assembled to achieve a real-time wire feeder adjustment according to the welding path. As shown in Fig. 5b), the rotation mechanism consists of a stator and a rotator. The stator, installed on the end-effector firmly, is hollow inside to enable the welding torch to pass through. The rotator is seated on the stator through a ball bearing, with a wire feeder tube and a motor positioned at two ends of the rotator, oppositely. In order to drive the rotator, a set of gears is fixed on the motor and stator, respectively. Thus, the rotation position and speed of the wire feeder tube can be adjusted according to the pre-defined welding path in real-time by controlling the motor. Because the rotation mechanism is attached to the welding torch directly, the direction adjustment of the wire feeder is independent and does not rely on the movement of the macro or the mini manipulator, which increases the flexibility of the system in confined spaces.

2.4.3. Control algorithm of the macro-mini collaborative manipulator system

Due to the independent movement of the welding torch, a synchronisation algorithm between the mini manipulator and the macro manipulator is required to achieve a collaborative welding task. For the control and synchronisation of the two motors, a National Instruments (NI) Field Programmable Gate Array (FPGA) board is adopted and connected to the two motors through two motor servo controllers, respectively. NI LabVIEW is used as the human-machine interface to send commands to both macro and mini manipulators synchronously (Fig. 6). Based on the hardware specifications, a communication frequency of 20 Hz is employed for the macro-mini manipulator system, which satisfies the requirement for a welding speed of 1 mm/s.

The synchronisation between the macro manipulator and the mini manipulator can be implemented by running an optimisation problem of an 8-DoF redundant robot with constraints on the joint movement limits (e.g., range and speed, etc.) and geometrical constraints of the working space while the objective function of the optimisation problem will include deviation from the desired path and robot energy, etc. The optimisation approaches of redundant robots have already been explained and explored in the current literature [21,22,23]. Thus, the paper focuses on the novelty of the mini manipulator design and kinematic modelling.

3. Modelling of the mini manipulator

For the collaboration between the mini manipulator and the off-the-shelf robot (macro manipulator) to perform non-time-dependent processes (e.g., drilling machining), the main concern is to control the Tool Centre Point (TCP) position accurately [24]. However, an additional challenge emerges when utilising the mini manipulator for time-dependent processes where any variation in speed will influence the final machining quality [25]. Therefore, in this case, two factors take

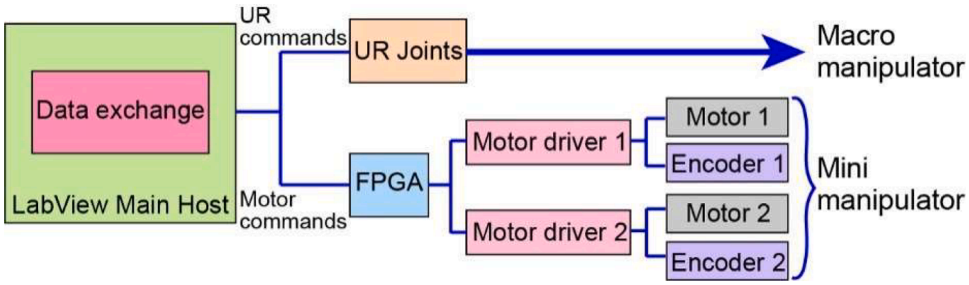

Fig. 6. Control architecture for the macro-mini collaborative manipulator.

the main responsibility for accomplishing a successful TIG welding task, i.e., welding torch TCP position as well as its speed [26]. Therefore, two parts of modelling are included in this section to fulfil the accuracy requirements of both position and speed of welding torch TCP based on the proposed design, i.e., kinematic modelling and Jacobian modelling. The kinematic modelling is required to achieve the predefined welding path (i.e., welding torch head TCP) by calculating the motor commands for the mini manipulator. Jacobian modelling is required to adjust the motor commands to achieve the desired TCP speed for the mini manipulator.

3.1. Kinematic modelling based on the design of the novel mini manipulator

To achieve a predefined welding path (i.e., welding torch head TCP), the motor commands should be calculated based on inverse kinematics. Therefore, kinematic modelling introduced in this section reveals the relationship between motor commands and welding torch TCP, which can be achieved by finding the following two relationships:

1) The relationship between the welding torch TCP and rotation angles of the two rotational cranks.
2) The relationship between rotation angles of the two rotational cranks and motor commands of the two motors.

3.1.1. Welding torch TCP and rotational cranks angles relationship

As shown in Fig. 7a), according to the kinematic chains of the mini manipulator, three coordinate frames, i.e., $O_wX_wY_wZ_w$(world frame), $O_LX_LY_LZ_L$ (LSC local frame) and $O_UX_UY_UZ_U$ (USC local frame), are established on the manipulator base, LSC and USC pivot axes, respectively. The pivot axes of LSC mechanism and USC mechanism are perpendicular to each other, with an offset distance of h, as shown in Fig. 7b). Therefore, the transformation matrix $\boldsymbol{T}_L^U$ of USC local frame relative to the world frame is as follows:

$$\begin{aligned}\boldsymbol{T}_L^U &= \boldsymbol{T}_L\cdot\boldsymbol{T}_{offset}\cdot\boldsymbol{T}_U \\ &= \begin{pmatrix}\cos\theta_1 & 0 & \sin\theta_1 & 0\\ 0 & 1 & 0 & 0\\ -\sin\theta_1 & 0 & \cos\theta_1 & 0\\ 0 & 0 & 0 & 1\end{pmatrix}\cdot\begin{pmatrix}1 & 0 & 0 & 0\\ 0 & 1 & 0 & 0\\ 0 & 0 & 1 & h\\ 0 & 0 & 0 & 1\end{pmatrix}\cdot\begin{pmatrix}1 & 0 & 0 & 0\\ 0 & \cos\theta_2 & -\sin\theta_2 & 0\\ 0 & \sin\theta_2 & \cos\theta_2 & 0\\ 0 & 0 & 0 & 1\end{pmatrix} \\ &= \begin{pmatrix}\cos\theta_1 & \sin\theta_1\sin\theta_2 & \sin\theta_1\cos\theta_2 & h\sin\theta_1\\ 0 & \cos\theta_2 & -\sin\theta_2 & 0\\ -\sin\theta_1 & \cos\theta_1\sin\theta_2 & \cos\theta_1\cos\theta_2 & h\cos\theta_1\\ 0 & 0 & 0 & 1\end{pmatrix}\end{aligned} \tag{1}$$

where $\boldsymbol{T}_L$ and $\boldsymbol{T}_U$ are homogeneous transformation matrices of the local frame O_L and O_U by rotating their circular crank with rotation angles of θ_1 and θ_2 along with local axis Y_L and axis X_U, respectively; $\boldsymbol{T}_{offset}$ is the homogeneous transformation matrix of the offset between the local frames O_L and O_U.

Assuming that the length of the welding torch in the local frame O_U is p and the welding torch TCP coordinates in the local frame O_U is $\boldsymbol{P}_{tip} = [0 \quad 0 \quad p \quad 1]^T$, it's coordinate $\boldsymbol{P}_w = [x \quad y \quad z \quad 1]^T$ in the world frame O_w can be generated by the kinematic chain of the mini manipulator as:

$$\boldsymbol{P}_w = \boldsymbol{T}_L^U\cdot\boldsymbol{P}_{tip} \tag{2}$$

By simplifying (Eq. (2)), the relationship between the welding torch TCP and rotation angles of the two circular cranks in the world coordinate frame is as follows:

$$\begin{cases} x = p\cdot\sin\theta_1\cos\theta_2 + h\cdot\sin\theta_1 \\ y = -p\cdot\sin\theta_2 \\ z = p\cdot\cos\theta_1\cos\theta_2 + h\cdot\cos\theta_1 \end{cases} \tag{3}$$

Based on the practical configuration of the mini manipulator, the rotational angles of θ_1 and θ_2 are in the range of $\left[-\frac{\pi}{18}, \frac{\pi}{18}\right]$. Therefore, the inverse kinematics between the rotation angles of the two rotational cranks and the welding torch TCP position can be calculated based on

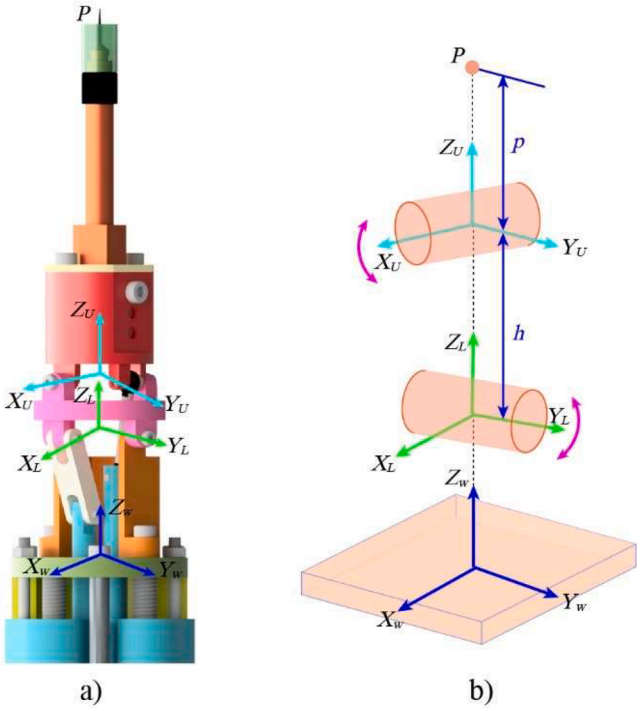

Fig. 7. The coordinate frames and the kinematic chain of the mini manipulator. a) three coordinate frames are established, i.e., world frame $O_wX_wY_wZ_w$ on the manipulator base, a local frame $O_LX_LY_LZ_L$ on the LSC pivot axis and a local frame $O_UX_UY_UZ_U$ on the USC pivot axis; b) The configuration of LSC and USC pivot axes is in perpendicularity with an offset distance of h.

(Eq. (3)) as:

$$\begin{cases} \theta_1 = \sin^{-1}\left(\dfrac{x}{h+\sqrt{p^2-y^2}}\right) \\ \theta_2 = -\sin^{-1}\left(\dfrac{y}{p}\right) \end{cases} \tag{4}$$

3.1.2. Rotational cranks angles and motors commands relationship

According to the mini manipulator configuration, the rotation angles of the two circular cranks (i.e., θ_1 and θ_2) are driven by two motors via LSC and USC linkages. The 3D model of the LSC linkage is shown in Fig. 8a) and its kinematic diagram is shown in Fig. 8b) to describe the movement relationship of the slider-crank linkage, where the translational movement of the slider driven by the motor is transformed into the rotational movement of the rotational crank through the slider and the link rod. As shown in Fig. 8c), a simplified version of the kinematic diagram is used to show the relationship between the rotation angle θ_1 of the circular crank and the displacement L_1 of the slider. For the right triangle $\Delta A_1C_1B_1$, its two catheti $\overline{A_1C_1}$ and $\overline{B_1C_1}$, can be represented as:

$$\begin{cases} \overline{A_1C_1} = L_1 - l_{12}\sin\theta_1 \\ \overline{B_1C_1} = l_{12}\cos\theta_1 - l_{10} \end{cases} \tag{5}$$

where l_{12} denotes the distance between the crank joint and the pivot; l_{10} denotes the offset distance of the slider to the Z-axis.

Therefore, by solving the right triangle ΔACB based on (Eq. (5)), the relationship between the rotation angle θ_1 of the circular crank and the displacement L_1 of the slider can be achieved as:

$$L_1 = \sqrt{l_{11}^2 - (l_{12}\cos\theta_1 - l_{10})^2} + l_{12}\sin\theta_1 \tag{6}$$

where l_{11} denotes the length of the link rod.

For the USC linkage, the rotation pivot is moving in real-time caused by the rotation of the LSC crank, which makes the kinematics much more complicated, as shown in Fig. 9a). Therefore, the slider displacement is not only related to the USC rotation angle but also related to the LSC rotation angle. To solve the kinematics of the USC linkage, the coordinate of the linkage endpoint $\boldsymbol{A}_2 = (0,\ l_{22},\ 0,\ 1)^T$ in the world frame needs to be calculated based on the transformation matrix $\boldsymbol{T}_L^U$ in (Eq. (1)).

Therefore, the endpoint $\boldsymbol{A}_2$ in the world frame is as:

$$(A_{2x},\ A_{2y},\ A_{2z},\ 1)^T = \boldsymbol{T}_L^U \cdot \boldsymbol{A}_2 \tag{7}$$

(Eq. (7)) can be simplified as:

$$\begin{cases} A_{2x} = l_{22}\sin\theta_1\sin\theta_2 + h\sin\theta_1 \\ A_{2y} = l_{22}\cos\theta_2 \\ A_{2z} = l_{22}\cos\theta_1\sin\theta_2 + h\cos\theta_1 \end{cases} \tag{8}$$

According to Fig. 9b and c), the USC linkage is projected to YOZ plane and XOZ plane, respectively. Therefore, the relationship between the slider displacement and the endpoint $\boldsymbol{A}_2$ is as:

$$(A_{2y} - l_{20})^2 + (A_{2z} + L_2)^2 = l_{21}^2 - A_{2x}^2 \tag{9}$$

By solving (Eq. (9)), the relationship between the slider displacement and crank rotation angles θ_1 and θ_2 can be represented as:

$$L_2 = \sqrt{l_{21}^2 - (l_{22}\sin\theta_1\sin\theta_2 + h\sin\theta_1)^2} - (l_{22}\cos\theta_2 - l_{20})^2 - (l_{22}\cos\theta_1\sin\theta_2 + h\cos\theta_1) \tag{10}$$

Therefore, by combining (Eqs. (4), (6) and (10)), the inverse kinematics of the mini manipulator is achieved as (Eq. (11)), and the motor commands can be calculated in real-time based on the welding torch TCP in the world coordinate.

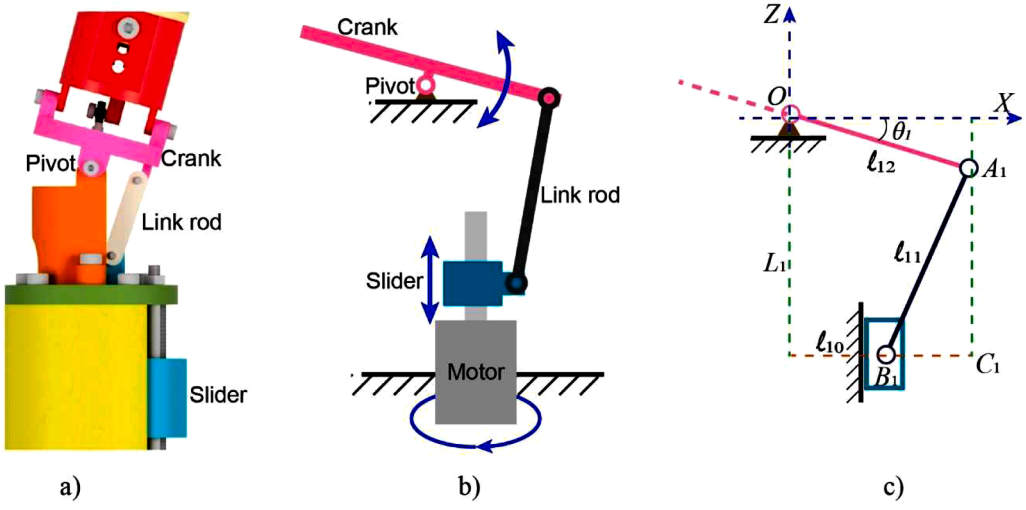

Fig. 8. Kinematic model of LSC linkage in the mini manipulator. a) a 3D model of the slider-crank linkage; b) a kinematic diagram of the LSC linkage which transforms the translational movement of the slider carried by the motor to the rotational movement of the circular crank; c) A simplified kinematic diagram of the LSC linkage to show the relationship between the rotation angle θ_1 of the circular crank and the displacement L_1 of the slider.

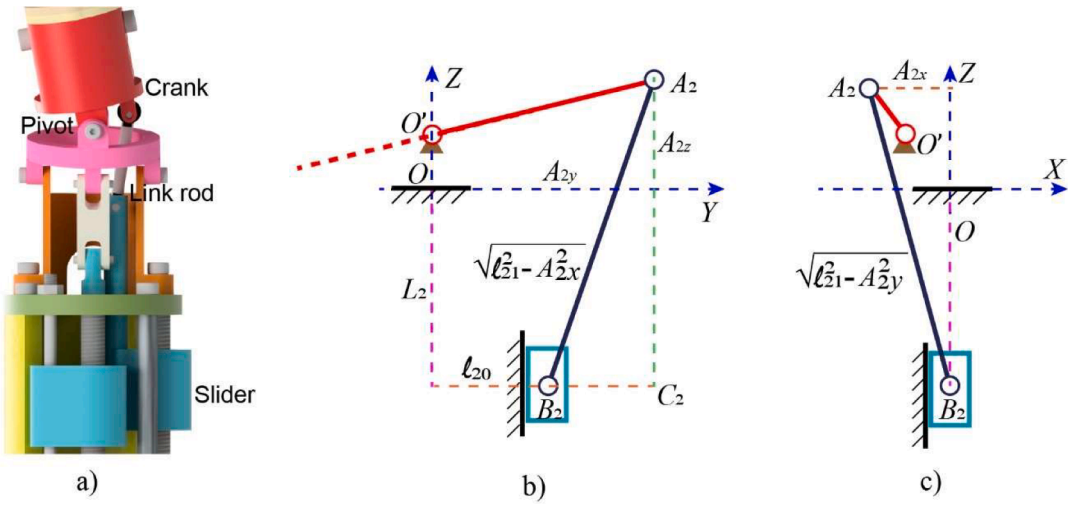

Fig. 9. Kinematic model of the USC linkage. a) 3D model of the slider-crank linkage; b) A simplified kinematic diagram of the USC linkage to show the relationship between the rotation angle θ_1, θ_2 and the displacement L_2 in the YOZ plane; c) A simplified kinematic diagram of the USC linkage to show the relationship between the rotation angle and the slider displacement L_2 in the XOZ plane.

$$\begin{cases} L_1 = \sqrt{l_{11}^2 - (l_{12}\cos\theta_1 - l_{10})^2} + l_{12}\sin\theta_1 \\ L_2 = \sqrt{l_{21}^2 - (l_{22}\sin\theta_1\sin\theta_2 + h\sin\theta_1)^2 - (l_{22}\cos\theta_2 - l_{20})^2} - (l_{22}\cos\theta_1\sin\theta_2 + h\cos\theta_1) \\ \theta_1 = \sin^{-1}\left(\dfrac{x}{h + \sqrt{p^2 - y^2}}\right) \\ \theta_2 = -\sin^{-1}\left(\dfrac{y}{p}\right) \end{cases} \tag{11}$$

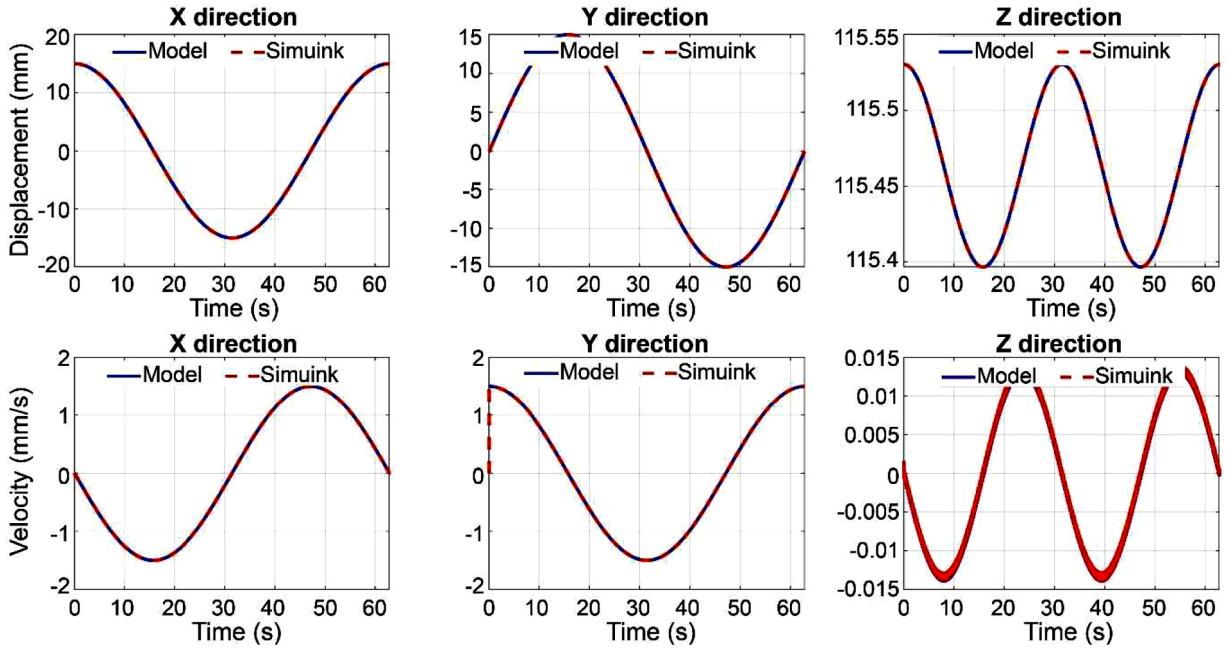

Fig. 10. Validation of kinematic and Jacobian modelling of the mini manipulator in MATLAB Simulink.

3.2. Jacobian modelling of the mini manipulator

For the welding process, both the TCP position and velocity play important roles in the final welding quality. Controllable TCP velocity can help the welding torch achieve a better and smoother welding path. Hence, the Jacobian matrix is achieved by differentiating (Eq. (3)), which reveals the velocity relationship between the welding torch TCP $\boldsymbol{V} = (\dot{x} \quad \dot{y} \quad \dot{z})^T$ and the two rotational cranks.

$$\begin{pmatrix} \dot{x} \\ \dot{y} \\ \dot{z} \end{pmatrix} = \begin{bmatrix} p\cos\theta_1\cos\theta_2 + h\cos\theta_1 & -p\sin\theta_1\sin\theta_2 \\ 0 & -p\cos\theta_2 \\ -p\sin\theta_1\cos\theta_2 - h\sin\theta_1 & -p\cos\theta_1\sin\theta_2 \end{bmatrix} \begin{pmatrix} \dot{\theta}_1 \\ \dot{\theta}_2 \end{pmatrix} \tag{12}$$

where $\boldsymbol{J}_1 = \begin{bmatrix} p\cos\theta_1\cos\theta_2 + h\cos\theta_1 & -p\sin\theta_1\sin\theta_2 \\ 0 & -p\cos\theta_2 \\ -p\sin\theta_1\cos\theta_2 - h\sin\theta_1 & -p\cos\theta_1\sin\theta_2 \end{bmatrix}$ is the Jacobian matrix between the TCP velocities of the welding torch and the rotation velocities of the two rotational cranks.

(Eq. (12)) can be abbreviated as:

$$V = \boldsymbol{J}_1 \cdot \dot{\boldsymbol{\theta}} \tag{13}$$

Similarly, the Jacobian matrix $\boldsymbol{J}_2$ is achieved by differentiating (Eqs. (6) and (10)), which reveals the relationship between the translational velocities of the two sliders $\dot{\boldsymbol{L}} = (\dot{L}_1 \quad \dot{L}_2)^T$ and the rotation velocities $\dot{\boldsymbol{\theta}} = (\dot{\theta}_1 \quad \dot{\theta}_2)^T$ of the two rotational cranks.

$$\dot{\boldsymbol{L}} = \boldsymbol{J}_2 \cdot \dot{\boldsymbol{\theta}} \tag{14}$$

Therefore, the relationship between the TCP velocities of the welding torch and the translational velocities of the two sliders can be determined by combining (Eqs. (13) and (14)) as:

$$V = \boldsymbol{J}_1 \cdot \left(\boldsymbol{J}_2^T \cdot \boldsymbol{J}_2\right)^{-1} \cdot \left(\boldsymbol{J}_2^T \cdot \dot{\boldsymbol{L}}\right) \tag{15}$$

3.3. Kinematic and Jacobian model validation via MATLAB simulation with CAD model

The verification of kinematic and Jacobian models is conducted in MATLAB Simulink, which is created by importing the CAD (Computer Aided Design) model of the mini manipulator into MATLAB. Thus, the Simulink environment can present all the design dimensions and joints of the mini manipulator. In the simulation, the mini manipulator is given a pre-defined circle path with a diameter of 15 mm. For the verification

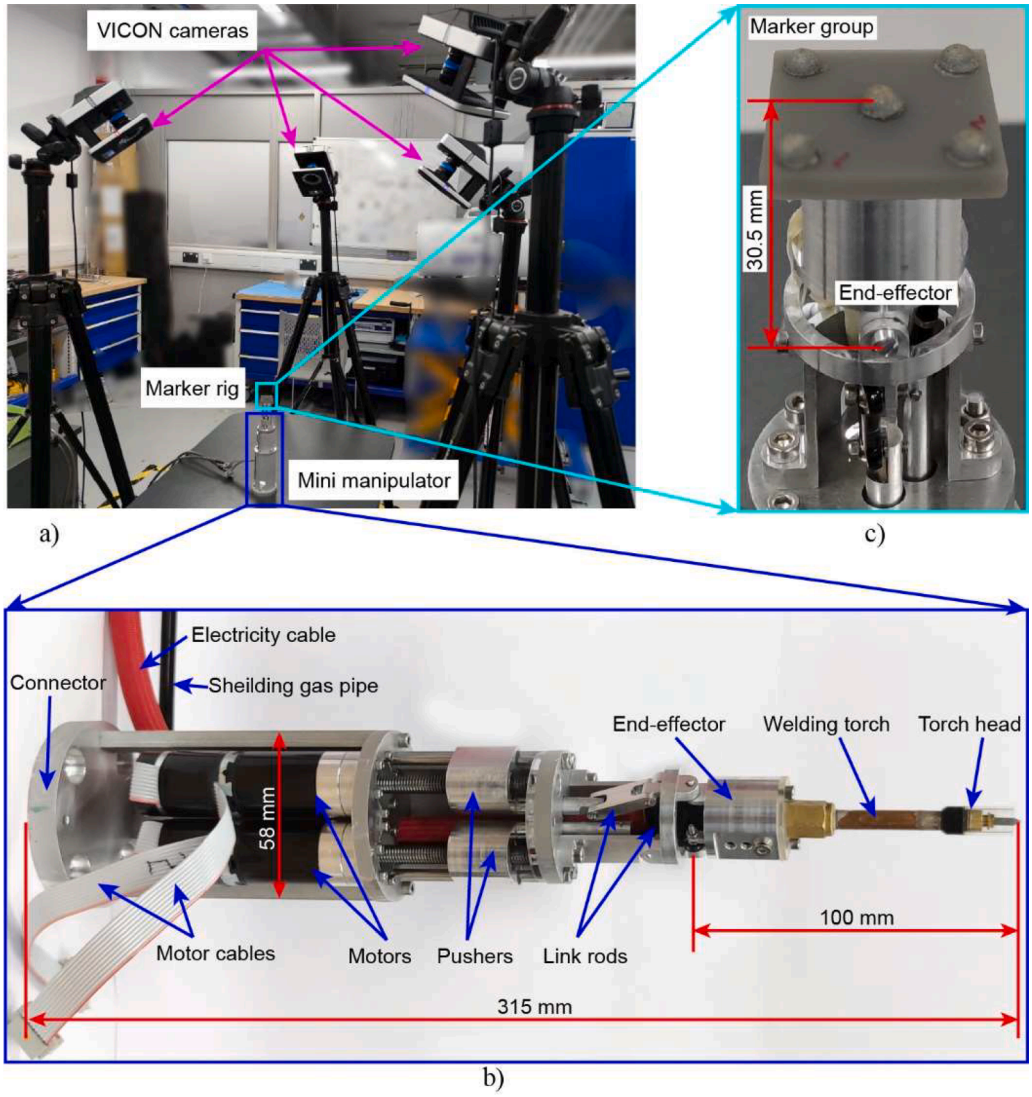

Fig. 11. Accuracy tests of the mini manipulator with VICON motion capture system. a) Experiment setup with the motion capture system consisting of four VICON cameras; b) detail view of the mini manipulator with torch head installed (during the test process, the torch head is replaced with a marker rig); c) detail view of the marker rig which consists of 5 retroreflective markers.

of the kinematic model, the displacements L_1 and L_2 of both sliders are calculated based on (Eq. (11)). Then the calculated slider displacements are sent to the Simulink model to generate the simulated TCP position, as shown in Fig. 10. The results of the simulated TCP position and desired TCP position are coincident with each other, which verifies the correctness of the kinematic model. For verification of the Jacobian model, the desired TCP velocities calculated by (Eq. (15)) are compared with the simulated velocities from MATLAB Simulink. As shown in Fig. 10, the results from simulated TCP velocities and desired TCP velocities are coincident with each other as well.

4. Experimental validation of the macro-mini collaborative manipulator

4.1. Accuracy tests by using a motion capture system

Although the simulation process has demonstrated the kinematic and Jacobian model of the mini manipulator, movement accuracy should also be explored considering that there are manufacturing and assembly errors, e.g. joint clearance. Therefore, a motion capture system (VICON camera system) is adopted to explore the movement accuracy of the mini manipulator after manufacturing and assembly, as shown Fig. 11. As shown in Fig. 11a), four Vicon motion capture cameras are strategically positioned to face the mini manipulator, ensuring that the movements of the mini manipulator's end-effector remain within the field of view of the four cameras. As detailed in Fig. 11b), the prototype of the mini manipulator is manufactured and assembled. The size of the mini manipulator prototype is 58 mm in diameter and 315 mm in length (with the welding torch head installed). It's worth noting that the dimension of the mini manipulator can be optimised and reduced based on the target application (e.g., using linear compact motors, frame-less motors or structure optimisation, etc.). However, during the accuracy test process, the welding torch are replaced with a marker rig, which is installed directly on the end-effector to eliminate the installation error. As shown in Fig. 11c), the marker rig comprises five hemispherical facial markers designed to reflect light emitted by Vicon cameras, with the reflected light subsequently captured by these cameras. During the movement of the mini manipulator, the Vicon cameras continuously monitor the marker rig in real-time at a frequency of 30 Hz. Consequently, the three-dimensional position and orientation of the mini manipulator's end-effector are estimated based on the detected positions of the markers by the Vicon cameras.

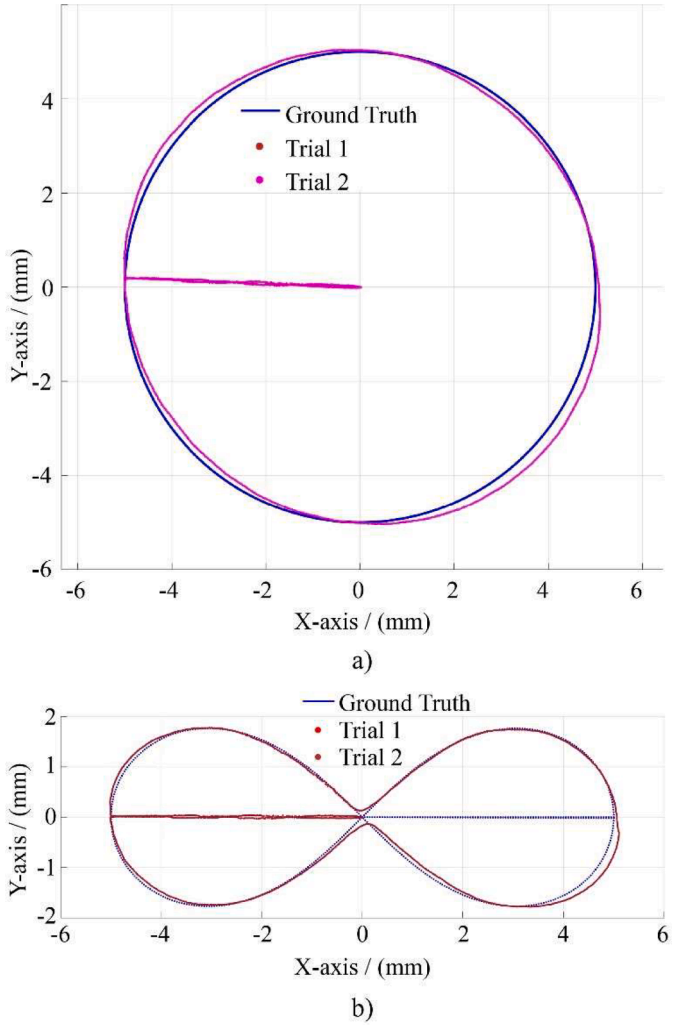

Fig. 12. Accuracy tests with different desired path. a) Circle path with a TCP speed of 1 mm/s; b) Infinity path with a TCP speed of 1 mm/s.

Two different desired paths are designed to test the accuracy of the mini manipulator (i.e., circle shape path and infinity shape path). The mini manipulator is first commanded to follow a circle path with a diameter of 10 mm. For the kinematic accuracy test, the marker is attached to the end-effector directly to eliminate installation errors, as shown in Fig. 11c). Thus, the position of the measurement point is 30.5 mm relative to the USC (Upper Slider-Crank linkage) coordinate frame. Although the working ranges in the task space at the measurement point are $x,y \in [-5,\ 5]$ mm, the working ranges of the joint space cover the full joint limitations ($\theta_1,\theta_2 \in \left[-\frac{\pi}{18},\ \frac{\pi}{18}\right]$), according to the kinematics of the mini manipulator.

The test is repeated two times to validate the repeatability of the mini manipulator. As shown in Fig. 12a), the maximum error of the mini manipulator is around 0.5 mm. Similarly, the mini-manipulator then follows an infinite shape path with an X-span of 10 mm and a Y-span of 3.6 mm. As shown in Fig. 12b), the maximum error of the mini manipulator by following the infinity path is 0.3 mm. In the real welding, the welding tip position will increase to 100 mm with the welding torch head installed. Thus, the errors measured at the Vicon markers point will be amplified by a factor $100/30.5 = 3.28$ at the welding tip point during real welding tests. For the error sources of the mini manipulator, besides the errors from the manufacturing and assembly process, it is worth noting that there exists clearance in the ball joint used in the LSC linkage. The clearance of the ball joint introduces the kinematic errors for the movements of the mini manipulator, especially when the movement of the pusher changes its direction. However, for different trials in both circle path and infinity path tests, although there exists clearance for the ball joint, the mini manipulator still has high repeatability accuracy, which validates that the clearance has little impact on the repeatability accuracy. Furthermore, it is worth noting that the dimension of the welding footprint is larger than the position errors, which, to some degree, attenuates the impact of the position errors on the final welding profile. In the future, a high-precise ball joint will be customised and manufactured to eliminate errors from clearance. In addition, it should be also noted that the current control algorithm of the mini manipulator is an open-loop control based on motor encoders. Hence, the accuracy can be improved by integrating a closed-loop control strategy in the future. It worth noting that, the size and complexity of the mini manipulator will be increased if extra sensors or transducers are needed for the integration of the close-loop control, which will sacrifice its flexibility in constrained spaces. Thus, close-loop control may be suitable for space-insensitive environments compared with open-loop control system in the future.

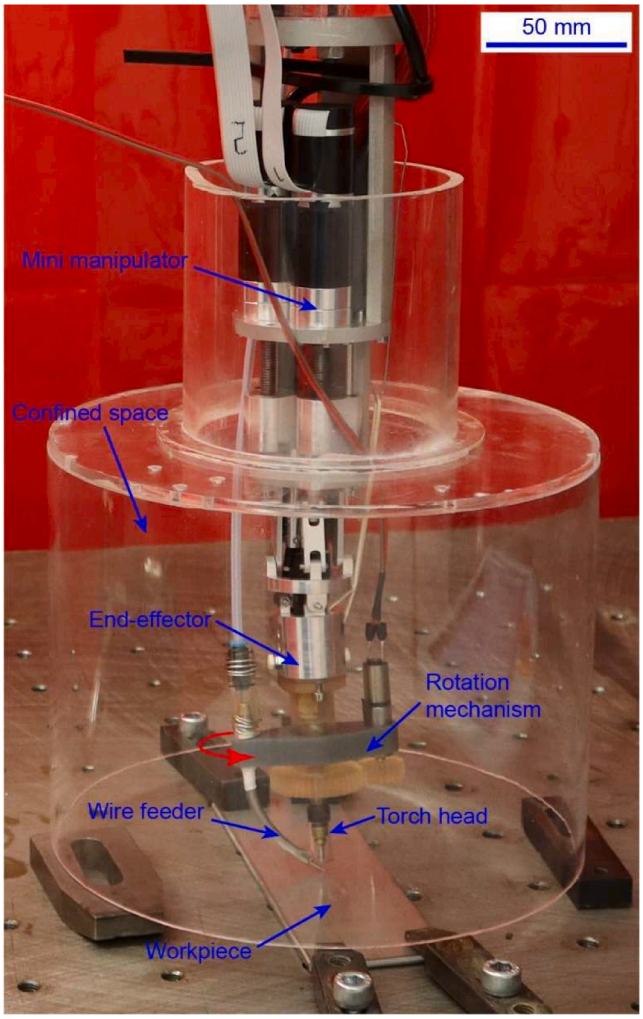

Fig. 13. Welding tests in confined pipe environments by using the proposed macro-mini manipulator system to follow a circle path on a horizontal surface.

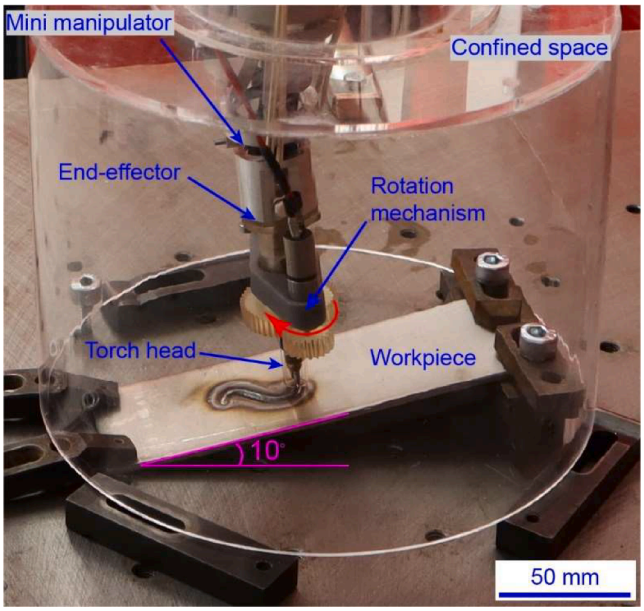

Fig. 15. Experiment setup of the collaborative macro-mini manipulator system to follow an S-shape path on an inclined surface.

4.2. *Validation of a collaborative system for welding in confined environments*

To demonstrate the feasibility of the macro-mini collaborative system, real welding tests are conducted with different pre-defined welding paths in confined spaces.

4.2.1. *Welding a circle path on a horizontal surface*

Firstly, the mini manipulator is commanded to follow a circle welding path with a diameter of 30 mm in a confined transparent pipe environment (this is for the convenience of observing the welding process). For this experiment setup, the macro manipulator carries the mini manipulator to access the confined pipe environment and arrive at the target workpiece to start the arc, as shown in Fig. 13. Because the mini manipulator itself can achieve a constant arc length by following a circle path on a horizontal surface, the macro manipulator keeps static during

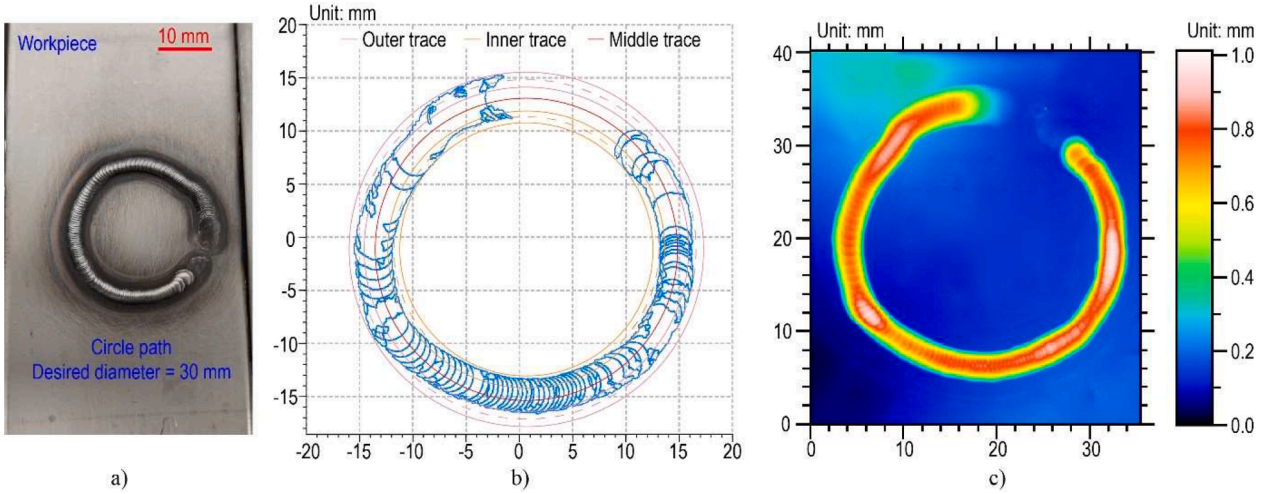

Fig. 14. Welding accuracy and quality analysis for the collaborative macro-mini manipulator system to follow a circle shape path. a) The final welding results for following a circle path; b) Contour of welding path shows the position accuracy of the collaborative welding system; c) Topography layer of the welding path shows the deposition height over the welding trace.

the welding process without providing compensation for the mini manipulator.

As mentioned before, when welding a circle path on a horizontal surface, there is no need for compensation from the macro manipulator. However, the macro manipulator is still required to carry the mini manipulator to access the confined environment and arrive at the target workpiece. As shown in Figs. 13 and 15, when arriving at the welding workpiece, the macro manipulator keeps static and the mini manipulator carries the welding torch to follow a circle path with a diameter of 30 mm and TCP velocity of 1 mm/s, following the commands sent by the LabVIEW and FPGA. During the welding process, the feeding direction of the wire feeder is adjusted by the rotation mechanism in real-time, which contributes to the success of the circle welding path. Three trials are repeated to show the repeatability performance of the mini manipulator.

To evaluate the welding quality of the macro-mini collaborative manipulator, a 3D Optical Profilometer (Bruker Alicona) is adopted to scan the welding paths to get the contour of the traces, as shown in Fig. 14a). For the contour of the welding profile depicted in Fig. 14b), the outer trace of the welding path is achieved by enclosing two circles (pink solid circles) and the diameter of the outer mean trace (pink dash circle) is calculated by averaging the diameters of the two circles (d_{OM} = 31.9 mm). Similarly, the diameter of the inner mean trace (brown dash circle line) is calculated by averaging the diameters of circles (brown solid circle line) enclosing the inner trace (d_{IM} = 24.9 mm). Finally, the mean diameter of the whole welding path can be calculated by averaging the outer mean trace and inner mean trace, according to (Eq. (16)).

$$d_M = \frac{d_{OM} + d_{IM}}{2} \tag{16}$$

where d_M denotes the mean diameter of the whole welding path; d_{OM} denotes the diameter of the outer mean trace; d_{IM} denotes the diameter of the inner mean trace.

In this case, the mean diameter of the welding path is 28.4 mm with the pre-defined welding path diameter of 30 mm. Thus, the relative error of the real welding trial is 5.3%, which is comparable with the relative error of 5.0% by using the VICON camera system. Furthermore, the highest deposition height of the welding path is around 0.9 mm and the width of the welding trace is around 3.5 mm, as shown in Fig. 14c).

4.2.2. *Welding an S-shape path on an inclined surface*

To further validate the collaborative mechanism with both macro and mini manipulators moving for the collaborative welding system, an S-shape path on an inclined surface is designed and tested, as shown in Fig. 15. For this experiment setup, the macro manipulator not only carries the mini manipulator to access the confined pipe space, but also provides compensation for the mini manipulator during the welding process. Based on the kinematics of the mini manipulator, although it can follow the S-shape path, the constant arc length cannot be ensured during the welding process. Therefore, the macro manipulator is required to provide compensation for the mini manipulator to achieve a constant arc length.

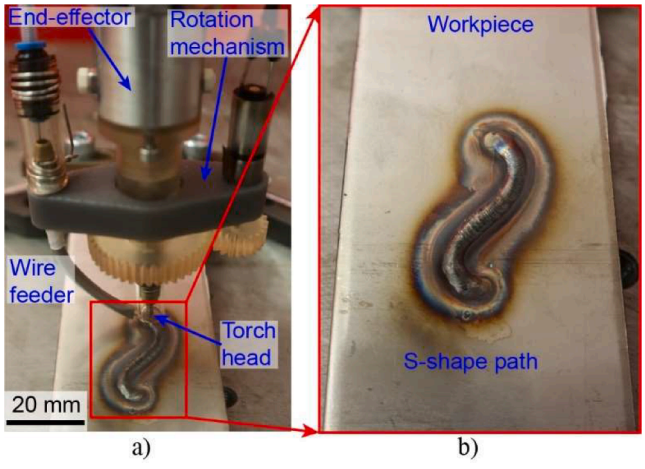

Fig. 16. Details and results for the collaborative macro-mini manipulator system to follow an S-shape path on an inclined surface. a) Detailed view of the end-effector and rotation wire feeder mechanism; b) The final welding results for following an S-shape path.

As shown in Fig. 16a), thanks to the compensation from the macro manipulator, the mini manipulator can ensure a constant arc length during the whole welding process without collision with the workpiece surface. This also validates the movement synchronisation between the macro manipulator and mini manipulator by the system control strategy. As shown in Fig. 16a), the rotation mechanism ensures that the wire feeder is always in the front of the welding feed direction, which is one of the factors that affect the success of TIG welding and final welding quality. As shown in Fig. 16b), the S-shape welding path on the inclined surface is successfully fulfilled by the collaboration of the macro manipulator and mini manipulator. Moreover, the synchronisation of the rotation mechanism with the collaborative manipulator system also contributes to the success of the S-shape welding path.

5. Conclusions

In this paper, a novel macro-mini collaborative welding system is proposed to achieve welding tasks in confined environments, which consists of a macro manipulator (universal robotic arm) and a novel mini manipulator. With the slim mini manipulator installed on the robot arm, the macro-mini collaborative manipulator system can achieve a (6 + 2)-DoF movement, which enables accessibility to confined environments with complex structures. In order to synchronise the macro manipulator and the mini manipulator, a control algorithm based on LabVIEW and FPGA is proposed and integrated into the welding system.

Furthermore, to fulfil a real-time wire feeder adjustment according to the welding direction, a rotation mechanism for the wire feeder is designed and attached to the welding torch. The width of the current wire feeder rotation mechanism is 63.5 mm, which is slightly larger than the body of the mini manipulator (58 mm). One reason is that an off-the-shelf stepper motor and a pair of 3D-printed gear sets are used to drive the wire feeder, which increases the size of the rotation mechanism. The other reason is that the welding wire is rigid so it needs a smooth bend tube rather than a sharp bend tube to achieve a successful wire delivery. For the first problem, the integration of a frameless motor to drive the system can reduce the size of the rotation mechanism. For the second problem, the integration of a localised heating system to soften the wire and help the wire pass a sharp bend tube will reduce the size of the rotation mechanism further. Both solutions will help decrease the size of the wire feeder rotation system in the future.

The proposed mini-manipulator is designed to fulfil 2-DoF motion for the end-effector in confined environments, which is actuated and achieved by two DC motors. To make the mini manipulator slim in the radial direction, the motors are moved to the bottom of the mini manipulator and two slider-crank linkages (i.e., LSC and USC) are used to connect the motors and the end-effector (i.e., welding torch) to accomplish 2-DoFs movements. Based on the novel concept and design of the mini manipulator, kinematic modelling including forward kinematics (FK) and inverse kinematics (IK) has been established. Furthermore, Jacobian modelling of the mini manipulator based on the Jacobian matrix has been achieved to explore the velocity relationship between the welding torch TCP and motor commands. What is more, a MATLAB Simulink simulation environment is created which validates the correctness of the kinematic and Jacobian modelling.

To further test the movement accuracy of the mini manipulator, a Vicon capture system is used to capture the end-effector movement of

the mini manipulator by following two pre-designed paths, i.e., circle path and infinity path. During the tests, the mini manipulator has a maximum error of 0.5 mm and 0.3 mm by following the circle path and the infinity path, respectively. For the error sources of the mini manipulator, besides the errors from the manufacturing and assembly process, it is worth noting that the current control algorithm of the mini manipulator is an open-loop control based on motor encoders. Hence, the accuracy can be improved by integrating a high-precise ball joint and a closed-loop control strategy in the future.

Finally, real welding tests are conducted with different welding paths in confined spaces, which demonstrate the feasibility of the macro-mini collaborative manipulator system. Firstly, welding a circle path on a horizontal surface in a confined pipe environment without compensation from the macro manipulator is used to demonstrate the welding ability of the mini manipulator. Then welding an S-shape on an inclined surface is adopted to demonstrate the compensation and collaboration ability of the macro-mini manipulator in confined spaces. The relative position error of the real welding trial is 5.3%, which demonstrates the advantage and practicability of the macro-mini collaborative manipulator system for welding in confined environments.

CRediT authorship contribution statement

Erhui Sun: Writing – review & editing, Writing – original draft, Visualization, Validation, Software, Methodology, Investigation, Formal analysis, Data curation, Conceptualization. **Josue Camacho-Arreguin:** Visualization, Validation, Software, Methodology, Investigation, Formal analysis, Conceptualization. **Junfu Zhou:** Validation, Methodology, Investigation. **Max Liebenschutz-Jones:** Visualization, Validation, Software, Methodology, Formal analysis. **Tianyi Zeng:** Writing – review & editing, Validation, Supervision, Software, Methodology, Investigation. **Max Keedwell:** Validation, Supervision, Investigation. **Dragos Axinte:** Writing – review & editing, Supervision, Resources, Project administration, Methodology, Investigation, Funding acquisition, Conceptualization. **Andy Norton:** Funding acquisition, Conceptualization. **Abdelkhalick Mohammad:** Writing – review & editing, Supervision, Resources, Project administration, Methodology, Investigation, Funding acquisition, Formal analysis, Conceptualization.

Declaration of competing interest

The authors declare the following financial interests/personal relationships which may be considered as potential competing interests: Abdelkhalick Mohammad and Dragos Axinte reports financial support was provided by UK Research and Innovation. D. Axinte, E. Sun, A. Madrigal, A. Mohammad, T. Zeng, M. Keedwell, J. Camacho Arreguin has patent Micromanipulator issued to US 20240149472. If there are other authors, they declare that they have no known competing financial interests or personal relationships that could have appeared to influence the work reported in this paper.

Acknowledgement

This work was supported and funded by UKRI Innovate UK project *REINSTATE* (Ref. 51689) and Rolls-Royce plc.

Supplementary materials

Supplementary material associated with this article can be found, in the online version, at doi:10.1016/j.rcim.2025.102975.

Data availability

No data was used for the research described in the article.

References

[1] B. Wang, S.J. Hu, L. Sun, T. Freiheit, Intelligent Welding System Technologies: State-of-the-Art Review and Perspectives, Elsevier B.V., 2020, https://doi.org/10.1016/j.jmsy.2020.06.020.
[2] Y.K. Liu, Y.M. Zhang, Supervised learning of human welder behaviors for intelligent robotic welding, IEEE Transact. Automat. Sci. Eng. 14 (3) (2017) 1532–1541, https://doi.org/10.1109/TASE.2015.2453351.
[3] A. Rout, B.B.V.L. Deepak, B.B. Biswal, Advances in Weld Seam Tracking Techniques for Robotic Welding: a Review, Elsevier Ltd., 2019, https://doi.org/10.1016/j.rcim.2018.08.003.
[4] Y. Xu, Z. Wang, Visual sensing technologies in robotic welding: recent research developments and future interests, Sens. Actuat. A Phys. 320 (2021) 112551, https://doi.org/10.1016/j.sna.2021.112551.
[5] Y. Huang, Y. Yuan, L. Yang, D. Wu, S. Chen, Real-time monitoring and control of porosity defects during arc welding of aluminum alloys, J. Mater. Process. Technol. 286 (2020) 116832, https://doi.org/10.1016/j.jmatprotec.2020.116832.
[6] W. Shen, T. Hu, C. Zhang, Y. Ye, Z. Li, A welding task data model for intelligent process planning of robotic welding, Robot. Comput. Integr. Manuf. 64 (September 2019) (2020) 101934, https://doi.org/10.1016/j.rcim.2020.101934.
[7] Y.K. Liu, Y.M. Zhang, Toward welding robot with human knowledge: a remotely-controlled approach, IEEE Transact. Automat. Sci. Eng. 12 (2) (2015) 769–774, https://doi.org/10.1109/TASE.2014.2359006.
[8] Y. Xu, et al., Welding seam tracking in robotic gas metal arc welding, J. Mater. Process. Technol. 248 (2017) 18–30, https://doi.org/10.1016/j.jmatprotec.2017.04.025.
[9] D. Axinte, Portable Robotised Machines Tools (RoboMach), for In-Situ Inspection and (re)manufacture: Research Challenges and Opportunities, Elsevier Ltd, 2024, https://doi.org/10.1016/j.ijmachtools.2024.104115.
[10] T. Lei, Y. Rong, H. Wang, Y. Huang, M. Li, A review of vision-aided robotic welding, Comput. Ind. 123 (2020) 103326, https://doi.org/10.1016/j.compind.2020.103326.
[11] Z. Mu, et al., Hyper-redundant manipulators for operations in confined space: typical applications, key technologies, and grand challenges, IEEE Trans. Aerosp. Electron. Syst. 58 (6) (2022) 4928–4937, https://doi.org/10.1109/TAES.2022.3217746.
[12] C.Y. Chen, J. Dai, G. Yang, C. Wang, Y. Li, L. Chen, Sensor-based force decouple controller design of macro–mini manipulator, Robot. Comput. Integr. Manuf. 79 (2023), https://doi.org/10.1016/j.rcim.2022.102415.
[13] A.E.K. Mohammad, J. Hong, D. Wang, Design of a force-controlled end-effector with low-inertia effect for robotic polishing using macro-mini robot approach, Robot. Comput. Integr. Manuf. 49 (2018) 54–65, https://doi.org/10.1016/j.rcim.2017.05.011.
[14] T. Olsson, et al., Cost-efficient drilling using industrial robots with high-bandwidth force feedback, Robot. Comput. Integr. Manuf. 26 (1) (2010) 24–38, https://doi.org/10.1016/j.rcim.2009.01.002.
[15] K. Kumar, C.S. Kumar, M. Masanta, S. Pradhan, A review on TIG welding technology variants and its effect on weld geometry, Mater. Today Proc. 50 (2021) 999–1004, https://doi.org/10.1016/j.matpr.2021.07.308.
[16] Q. Guo, et al., Progress, Challenges and Trends on Vision Sensing Technologies in Automatic/Intelligent Robotic Welding: State-of-the-Art Review, Elsevier Ltd, 2024, https://doi.org/10.1016/j.rcim.2024.102767.
[17] K.J. Waldron, J. Schmiedeler, Kinematics. Springer Handbook of Robotics, 2016, pp. 11–36.
[18] X.-J. Liu, J. Wang, Parallel kinematics. Springer Tracts in Mechanical Engineering, 2014.
[19] C.C. de Wit, B. Siciliano, G. Bastin, Theory of Robot Control, Springer Science & Business Media, 2012.
[20] D.A. Axinte et al., "Micromanipulator," US 20240149472, May 09, 2024.
[21] B. Siciliano, Kinematic control of redundant robot manipulators: a tutorial, J. Intell. Robot. Syst. 3 (3) (1990) 201–212, https://doi.org/10.1007/BF00126069.
[22] R.V. Patel, F. Shadpey, Control of Redundant Robot manipulators: Theory and Experiments, 316, Springer Science & Business Media, 2005.
[23] D. Chen, Y. Zhang, A hybrid multi-objective scheme applied to redundant robot manipulators, IEEE Transact. Automat. Sci. Eng. 14 (3) (2017) 1337–1350, https://doi.org/10.1109/TASE.2015.2474157.
[24] S. Garnier, K. Subrin, K. Waiyagan, Modelling of robotic drilling, in: Procedia CIRP, Elsevier B.V., 2017, pp. 416–421, https://doi.org/10.1016/j.procir.2017.03.246.
[25] Y. Mizoue, B. Sencer, A. Beaucamp, Identification and optimization of CNC dynamics in time-dependent machining processes and its validation to fluid jet polishing, Int. J. Mach. Tool. Manuf. 159 (2020), https://doi.org/10.1016/j.ijmachtools.2020.103648.
[26] H. Parmar, V. Nair, Review on investigate the TIG welding of aluminum by controlling parameter, Int. Res. J. Eng. Technol. (IRJET) (March) (2019) 349–354.